Convergence Analysis of an Iterative Targeting Method for Keyhole Robotic Surgery

Short Communication

Mirko Daniele Comparetti[1,*], Elena De Momi[1], Tim Beyl[2],
Mirko Kunze[2], Jörg Raczkowsky[2] and Giancarlo Ferrigno[1]

1 NeuroEngineering and Medical Robotics Lab, Department of Electronics, Information and Bioengineering, Politecnico di Milano, Milan, Italy
2 Robotics and Automation Laboratory (IPR), Institute for Antropomatics and Robotics, Karlsruhe Institute of Technology, Karlsruhe, Germany
* Corresponding author E-mail: mirkodaniele.comparetti@polimi.it

Abstract In surgical procedures, robots can accurately position and orient surgical instruments. Intraoperatively, external sensors can localize the instrument and compute the targeting movement of the robot, based on the transformation between the coordinate frame of the robot and the sensor.

This paper addresses the assessment of the robustness of an iterative targeting algorithm in perturbed conditions. Numerical simulations and experiments (with a robot with seven degrees of freedom and an optical tracking system) were performed for computing the maximum error of the rotational part of the calibration matrix, which allows for convergence, as well as the number of required iterations.

The algorithm converges up to 50 degrees of error within a large working space.

The study confirms the clinical relevance of the method because it can be applied on commercially available robots without modifying the internal controller, thus improving the targeting accuracy and meeting surgical accuracy requirements.

1. Introduction

Robotic assistants can increase the accuracy and repeatability of an intervention [1], for instance, when positioning surgical tools on target poses (i.e. targeting), defined by medical images during preoperative planning. When multiple probe insertions are required, such as in neurosurgery (deep brain stimulation or stereoelectroencephalography (SEEG)), or in prostate brachytherapy, robotic targeting allows one to avoid manoeuvres involving the stereotactic frame [2] and to avoid using fixed grid-based trajectories (e.g., in SEEG or prostate brachytherapy).

Targeting accuracy requirements depend on the clinical application. Furthermore, it is necessary to distinguish between the technical and the clinical accuracy achieved.

The technical accuracy of frame-based stereotactic procedures is about 0.05 mm, while frameless stereotaxy has a technical accuracy of lower than 0.5 mm. In both cases, the accuracy achieved in clinical practice is far worse than the level of technical accuracy.

In neurosurgical keyhole procedures [7], where access to the brain is via an entry point of about 5 mm in diameter, the clinical positioning accuracy of straight probes at the entry point has to be below 1 mm [8]. The same targeting accuracy is required in ear, nose and throat interventions [9], where robotic drilling guides can be used to perform cochleostomy [10]. In Table 1, the technical and clinical accuracy values of commercially available robotic systems are reported.

Robot	Clinical accuracy	Technical accuracy
SpineAssist	1 mm [6]	0.1 mm [5]
Neuromate	0.82 mm to 2.9 mm [21]	--
Robodoc	1 mm [11]	--
Cyberknife	1.1 mm [13]	--
SABiR	--	0.4 mm [31]
Pathfinder	1 mm [32]	0.5 mm to 2.7 mm [21], [22]
MAKOplasty	3° [12]	--
Rosa	--	0.90 mm ± 0.3 mm (specs)

Table 1. Surgical robot accuracy

In image-guided robotic surgical procedures, as for all image-guided procedures, a registration defines the geometrical transformation between the preoperative plan and the intraoperative environment in which the task is defined. The ROBODOC® system (Curexo Technology Corporation, Fremont, Canada) [11] and the MAKOplasty® (MAKO Surgical Corp, Fort Lauderdale, USA) [12], used in orthopaedic procedures, are both registered to the intraoperative environment by touching pins screwed in the bones, visible in preoperative CT images. This positions the robot's tool centre point (TCP) on the pin's tip. Intraoperative X-ray images are used for the target registration in the Cyberknife® system (Accuray Inc., Sunnyvale, California, USA) [13], which is used for radiosurgery procedures. Similarly, the Neuromate® system (Renishaw Ltd., UK), used to position electrodes in the brain for stereo-electroencephalography (SEEG), is registered to the intraoperative target (the patient's head) using intraoperative fluoroscopic images. Surface matching techniques are used for the registration of the intraoperative scenario with the preoperative world, using, for example, the ROSA (Medtech, France) system.
A calibration procedure estimates the transformation between the coordinate frame (CF) of the surgical tool attached to the robot's end effector (EE) (e.g., the probe or the cutting guide) and the TCP itself. If an external sensor, e.g., an optical localizer, is used, the calibration

procedure estimates the geometrical transformation between its CF and the robot's CF. Such calibration [14] can be performed with closed form solutions [15] or with iterative optimization approaches [16–18]. In robotic surgery, external sensors can also allow the definition of the task in the robot's coordinate frame and can also check the accuracy of the task during its execution. External position sensors can also be used for iteratively correcting the pose of the robot when deviations between the actual and the planned pose are detected [19, 20]. They can also be used to register the intraoperative reality on the preoperative images [29], thus allowing the surgical tool's navigation and enabling compensation for patient motion in several medical applications. Such deviations happen because serial robots have low absolute accuracy due to the fact that robots' models are inaccurate [21, 22], but also because the calibration between the robot's space and the measurement system is affected by errors [18]. Moreover, external sensors in the operating room can be used to detect and compensate for possible motion during the intervention [23] or during trans-cranial magnetic stimulation in order to maintain the stimulating probe on the planned pose [24, 25].

Previously, we presented a closed-loop iterative algorithm for positioning and orienting a surgical tool in minimally invasive neurosurgery by using a multi-robot cell and an optical localization system as external sensor. This was intended to increase the targeting accuracy and to simplify the patient-robot registration procedure [20, 26]. The robot's task was defined in the optical CF and the robots automatically aligned the surgical probe to the target pose. Residual error transformations were iteratively corrected using a scaling factor. The targeting accuracy was experimentally computed in a neurosurgical mock-up scenario. The final targeting accuracy can be of the same order of magnitude as the external sensor, independent of the calibration accuracy, only by adopting iterative targeting. The aim of this paper is to provide simulated and experimental evidence of the robustness of iterative targeting convergence, with respect to perturbations in the calibration matrices, to robot pose and to the targeted point for a robot-aided keyhole neurosurgical procedure, such as brain biopsy or electrode placement.

2. Targeting convergence analysis

An iterative algorithm is used for compensating for targeting errors. Its robustness is understood to be the ability of such an algorithm to converge when starting from a perturbed initial condition and using perturbed data.

In a robot manipulator, the base CF (CF_{Base}) identifies the robot's internal reference frame and the TCP CF (CF_{TCP}) identifies the reference frame of free extremity. External

localization sensors (e.g., cameras, fluoroscopic images and localization systems [27]) can be used to track the robot's links. The transformation matrices X and Y, which relate to the position and orientation of the markers attached to the last link dynamic reference frame (DRF) with respect to the robot's CF_{TCP}, can be estimated with a "hand-eye" calibration procedure [14]. The procedure used in this paper is described in [18] and involves minimization techniques in order to solve the matrix system

$$A \cdot X = Y \cdot B \qquad (1)$$

in which the X and Y matrices are the calibration matrices, B is the robot pose (forward kinematics) and $A = G^{-1} \cdot T$ (Figure 1) is the transformation from the last link DRF and the robot base DRF, where G and T are the robot base and the robot tool poses in the localizer reference frame, respectively.

The surgical tools connected to the robot's last link (and to the actual robot's EE) are also calibrated with respect to the markers on the robot [20]. In the following, we assume that the CF of the surgical tool and the CF of the markers attached to the robot's last link are coincident.
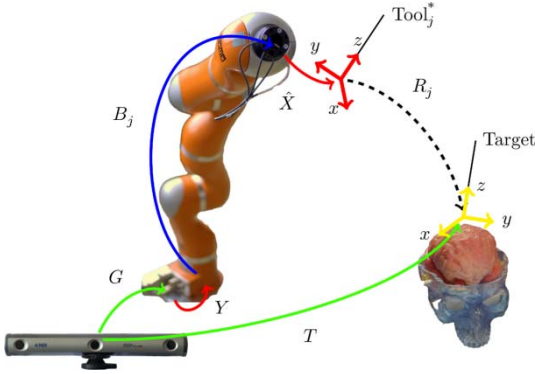

Figure 1. Targeting scenario; the tracking system (bottom left) localizes the tool and the target to the world (CF)
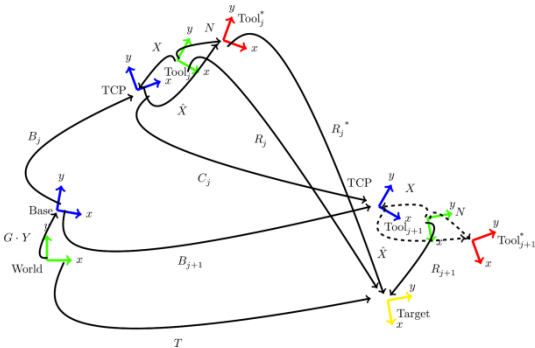

Figure 2. CFs and transformations: 'World' is the CF of the external sensor, 'Target' is the desired pose to be reached and 'Tool*' is the estimated CF of the tool; the arrows represent the geometrical transformations, j represents the time index and the variable marked with * are the ones obtained by estimation procedures.

Unknown transformations are:
- R_j^*: the transformation between the CF_{Tool^*} and the CF_{Target};
- X: actual transformation from the CF_{Tool} to the CF_{TCP} [14];
- $\hat{X}$: estimated transformation from the CF_{Tool^*} to the CF_{TCP} (calibration matrix) [14].

The relationship between $\hat{X}$ and X is:

$$\hat{X} = X^{-1} \cdot N \qquad (2)$$

where N is the error transformation due to the calibration inaccuracy. In order to align the estimated tool pose (CF_{Tool^*}) with the tool target pose (CF_{Target}), the robot pose has to change from B_j to B_{j+1} according to the estimated C_j transformation

$$B_{j+1} = B_j \cdot C_j \qquad (3)$$

where C_j is:

$$C_j = X \cdot R_j \cdot X^{-1} \qquad (4)$$

that is approximated with $\hat{C}_j$, computed as:

$$\hat{C}_j = \hat{X} \cdot R_j \cdot \hat{X}^{-1} \qquad (5)$$

in which X is approximated with $\hat{X}$. From this point on, $\hat{B}_{j+1} = B_j \cdot \hat{C}_j$ (approximating B_{j+1}) is consequently computed as:

$$\begin{aligned} \hat{B}_{j+1} &= B_j \cdot \hat{X} \cdot R_j \cdot \hat{X}^{-1} \\ &= B_j \cdot X^{-1} \cdot N \cdot R_j \cdot N^{-1} \cdot X \end{aligned} \qquad (6)$$

Targeting iterations are therefore needed to bring the tool CF to the tool target pose. Iterations are stopped when R_j translation and rotation components are both below a predetermined threshold value, chosen according to the application's requirements (1 mm in this instance) [4].

The targeting algorithm brings the surgical tool into the target pose T, with the robot in the initial pose B_0 (Figure 2). When the transformations N and R_j are pure translations, convergence is reached within one iteration:

$$\hat{B}_{j+1} = B_j \cdot X^{-1} \cdot R_j \cdot X = B_{j+1} \qquad (7)$$

When, instead, the transformation N is a not-nil rotation, the targeting iterates until the residual error transformation R_j is below a predefined threshold.

Targeting is iteratively performed, correcting the robot's EE pose in the Cartesian space; this is done by measuring the position reached by the tool after the movement is performed and by calculating the correction from the error with respect to the desired pose. This is performed

after the programmed movement of the robot. The rather long time required for robot movement, sensing and error correction allows for the neglect of the robot's dynamics.

3. Methods

Numerical simulations and laboratory experiments were performed to assess the targeting convergence with respect to the calibration error and the robot's initial pose. The robot's initial pose (the rotation and translation components of B_0, B_0^θ and B_0^d respectively[1]), the target pose (the rotation and translation components of T, T^θ and T^d respectively) and the calibration matrix were perturbed, as reported in Table 2. The calibration matrix X was multiplied by an error matrix N^θ. N^θ represents all the errors in the robot calibration chain which can be due to encoders, the external measurement system or calibration estimation inaccuracies.

The rotation component of the transformation matrices (N^θ, B_0^θ and T^θ) were rotations about the trisectrix of the first octant. The translation components of the transformation matrices, B_0^d and T^d, were along a vector obtained by rotating the x axis by 30° around the y axis and rotating the resulting vector by 30° around the x axis. The ranges and steps of variation are reported in Table 2.

Data	Range	Step (simulation)	Step (experiments)
N^θ	(0 to 60)°	0.25	10°
B_0^θ	(0 to 60)°	1°	6°
B_0^d	(0 to 150) mm	1 mm	15 mm
T^θ	(0 to 60)°	1°	6°
T^d	(0 to 150) mm	1 mm	15 mm

Table 2. Ranges of variation

The following parameters, which represent the metric of robustness, were estimated:

1. N_{MAX}^θ, which is the maximum angular component of N, which allows convergence as a function of B_0^θ, B_0^d, T^θ and T^d;
2. # iterations: the number of iterations for targeting, varying between N^θ, B_0^θ, B_0^d, T^θ and T^d. At N_{MAX}^θ, the correlation between the number of iterations and the variations of B_0 and T were computed using the Pearson correlation coefficient ($\alpha < 0.05$). The relationship between the number of iterations and the value of the N^θ component was fitted using an exponential function.

---

[1] The transformation matrix A has six degrees of freedom (DoFs): three coordinates x, y and z, defined as A^x, A^y and A^z, respectively, in addition to three rotation angles A^ϕ, A^ψ and A^ω around the three axis. The norm of the translation component (displacement) is $A^d = \sqrt{A^{x2} + A^{y2} + A^{z2}}$. The angle of rotation is the angular component A^θ of the quaternion q extracted from the rotation sub-matrix of A and is $A^\theta = 2 \cdot \arctan2\left(\frac{q_s}{\|q_v\|}\right)$.

In order to analyze the convergence of the targeting over a wide range of the perturbing parameters, numerical simulations were performed (MATLAB® R2012a, The MathWorks, Natick, Massachusetts, USA). X was assumed to be a 4×4 identity matrix. This allows rewriting eq. (6) as follows:

$$\hat{B}_{j+1} = B_j \cdot N \cdot R_j \cdot N^{-1} \tag{8}$$

The selected threshold of R_j, as the minimum positioning resolution, is 0.8 mm for the translation component and 0.05° for the rotation component, which allows for the satisfaction of neurosurgical applications' requirements [26]. The maximum number of permitted iterations was 100 and no measurement noise was added during the simulation.

The convergence performances of the algorithm were also experimentally tested using a KUKA 4+ lightweight robot (LWR) (KUKA Laboratories, Augsburg, Germany) with seven degrees of freedom (DoFs)[28] and the OptoTrack Certus optical tracking system (NDI, Ontario, Canada), with 0.15 mm stated accuracy, as external sensor. In 15 trials, the median technical accuracy for the robot, achieved while reaching a target fixed in space, was 1.18 mm (with 0.91 mm and 1.44 mm as first and third quartiles) and 0.95° (with 0.93° and 0.98° as first and third quartiles) for the translation and rotation components, respectively.

Two sensors (dynamic reference frames), each composed of four active markers, were attached to the robot's last link (end effector) and to the robot base. The robot and the tracking system reference frame were calibrated [14] and the X transformation estimated ($\hat{X}$).

The robot's target positions were varied as reported in Table 2 and the iterative algorithm convergence was assessed.

The selected threshold of R_j, as the minimum positioning resolution, is 0.8 mm for the translation component and 0.05° for the rotation component. The maximum number of permitted iterations was 100.

4. Results

The maximum angular component of N which allows convergence, N_{MAX}^θ, turned out to be independent of the B_0 and T variations. In simulations, the N_{MAX}^θ result was around 55° in the case of B_0^θ, 54.25° in the case of B_0^d and around 57.5° in the case of T variations (both angular and translation components). In experimental conditions, the N_{MAX}^θ result was 50° in the case of B_0 and T variations. The convergence extended up until $T^\theta = 42°$, since for $T^\theta \geq 42°$ the markers were not visible from the external sensor.
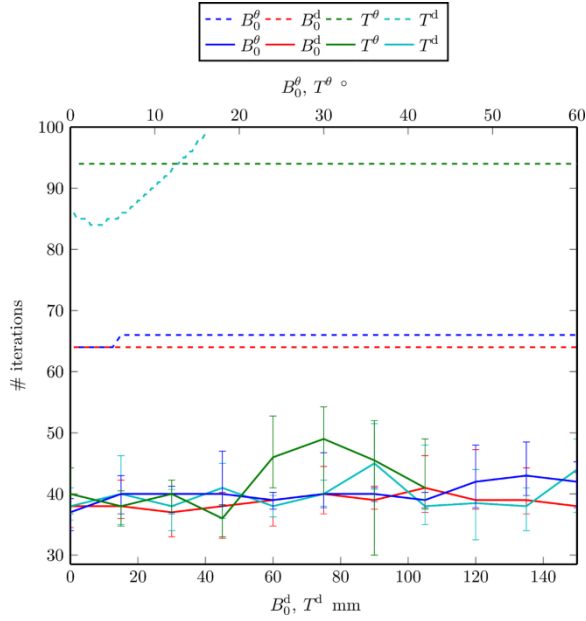
Figure 3. Number of iterations required for targeting convergence in simulation (dashed line) with $N^\theta = 57.5°$ and in experimental conditions (solid line, median and percentiles are also reported) with $N^\theta = 50°$.
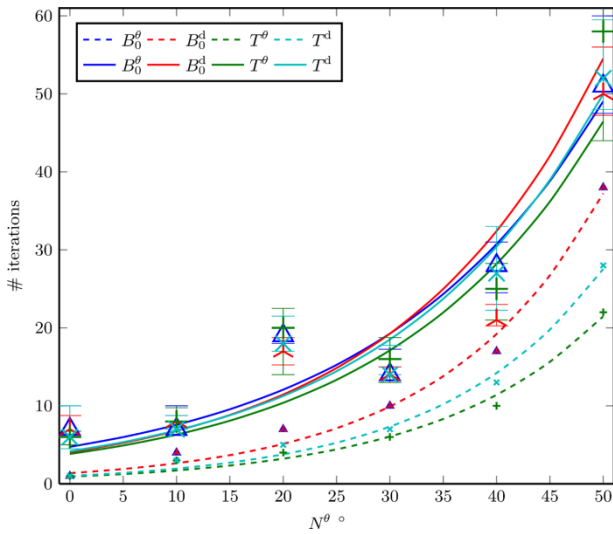

Figure 4. Maximum number of targeting iterations required as a function of N^θ, evaluated for all the possible B_0 and T variations. The lines are the exponential fitting of the data; the dashed lines are simulation results while solid lines are experimental results (with median and quartiles values).

In Figure 3, the number of targeting iterations is shown, as a function of B_0 and T, with $N^\theta = N^\theta_{MAX}$, which is higher in the simulation than in the experiments. In simulations, the number of iterations is independent of B_0 and T and is around 65 in case of B_0 variations and 95 in case of T^θ variations. In the set-up described in § 3.2, when T^d is greater than 40 mm, the algorithm does not converge within 100 iterations. In experiments, the number of required iterations is approximately 40 and is independent from B_0 and T variations. Convergence is achieved in about 80 iterations.

Figure 4 shows the maximum number of targeting iterations required as a function of N^θ, evaluated for all the possible B_0 and T variations. N^θ was varied until N^θ_{MAX}, i.e., 50°. As shown, the number of iterations increases exponentially in both testing conditions. Figure 4 further confirms the results shown in Figure 3: convergence was achieved in a finite number of iterations, until N^θ was around 55° in simulations and 50° in the case of experimental conditions.

5. Discussion

In keyhole procedures for neurosurgery, the accuracy of the positioning of the tool is crucial for the outcome of the procedure and the time required for the positioning of the tool is negligible. In those procedures, access to the brain is via to a small hole, causing a reduced loss of cerebrospinal fluid and reduced brain shift, minimizing the target's displacement. In keyhole surgery, where a straight tool (e.g., a probe) has to be accurately positioned, as defined in the preoperative plan, serial and parallel robots can be used. For example, neurosurgical interventions, such as deep brain stimulation or SEEG, require a targeting accuracy below 1.1 mm. Unfortunately, the accuracy of serial robots is limited due to possible manufacturing inaccuracies and to intrinsic system compliance issues. The reported accuracy values of serial robots are in the range of 0.5 mm to 4.4 mm [21, 22], while parallel robots' working space is reduced. The combined use of an accurate external sensor in robotic surgery is helpful because its positional accuracy, i.e., the accuracy of the measurement of the position and orientation of rigid bodies in space, is higher than the robot's accuracy. This allows for the measurement of discrepancies with respect to the desired pose.

The aim of this paper is to find a measurable perturbation in terms of calibration errors that allow us to define the robustness of the iterative targeting [20] with regard to such perturbation. Calibration inaccuracies can be due to noise in the measurement system or to robot inaccuracies. Previous work [17, 18] showed that hand-eye calibration errors are in the range of 0.06 mm for translation values and 0.03 rad for rotation values, which are two orders of magnitude less than the N^θ_{MAX} we computed. Independent of calibration, the targeting accuracy has to be less than 1 mm at the target point. We provided simulated and experimental evidence of convergence of the iterative robotic targeting algorithm for image-guided robotic surgery, with respect to perturbations of the calibrated transformation matrices between the robot and the external sensors, while varying the initial poses of both the instruments and the robot. The convergence of our iterative targeting provides assurance that the obtained accuracy is lower than the selected thresholds (0.8 mm and 0.05°) thus satisfying technical requirements

for neurosurgery. In our study, the selected convergence threshold is higher than that of the tracking system used in the experiments (3.2). Furthermore, it is of the same order of magnitude as the most accurate commercially available tracking systems. Moreover, that value was selected because it is of same order of magnitude as stereotactic frames (whose positioning accuracy can be influenced by the manual adjustments of the frame). It can also be lowered according to the technical accuracy of the external sensor used. The robotic positioning systems presented in the literature make it possible to achieve a targeting accuracy in clinical trials which is not better than the one selected in this work. For example, the ROBODOC® system allowed the positioning of the bone cutting guide with 1 mm error [11] and the Cyberknife® system allowed the orientation of the beam with 1.1 mm error [13]. The Neuromate® system allowed the performance of brain biopsies with 0.86 (± 0.32) mm accuracy [30]. The parallel robot presented in [31] was able to achieve 0.4 mm accuracy via kinematic calibration, which was obtained using an optical localizer and the targeting procedure with a closed-loop controller.

We simulated a calibration error which is two orders of magnitude greater than the calibration errors usually reported. We tested the convergence robustness. Simulations allowed for the testing convergence in a way that extensively explored the parameter space (B, T, N), more extensively than was possible with the experiments. It has to be acknowledged that we did not simulate any measurement noise. The targeting accuracy, experimentally computed in the same conditions, nonetheless satisfies the requirements for relevant interventions.

In our setup, the tool to be aligned to the target pose was considered to be coincident with the CF tracked by the external monitoring system. In the experiments, only the calibration rotation error was considered, since translations are corrected in a single iteration step. Also, the robot's initial pose (B_0) and the tool's target pose (T) were varied in range. This is compatible with operating room constraints, both in simulation and in experimental conditions. We showed that targeting convergence was reached independently from B_0 and T, for errors in the calibration matrix of up to 60° in the simulation and around 50° under experimental conditions. When the N_{MAX}^{θ} calibration matrix is multiplied, the number of iterations required to converge is almost independent of B_0 and T, both in simulations and experimental conditions (Figure 2a). In experimental conditions, fewer iterations are needed to reach the target since the N_{MAX}^{θ} value used was slightly inferior (50° instead of 60°). Finally, there is an exponential increase in the number of iterations when the N matrix rotation component is varied, both in simulation and in experimental conditions

(Figure 2b). For calibration errors of the same amplitude of the ones reported in the literature, the number of requested iterations is approximately 10, which is compatible with the neurosurgical intervention time. In fact, in each iteration the robot's movement takes about three seconds, which is a small amount of time for the overall process to reach the target compared to the total duration of the intervention, which is several hours.

For the experimental evaluation, we used a KUKA LWR, whose basic accuracy does not satisfy the surgical requirements. This robot features torque sensors in each joint, which increase the safety of the device, enabling it to detect collisions while making the structure more flexible than that of a classic industrial serial robot. It has a redundant kinematic structure, which enables the possibility of avoiding obstacles while keeping the end effector in its pose. This increases the space in which the robot can work with dexterity, making it more suitable for a crowded environment such as the operating room. The algorithm we present can also be integrated with other environmental sensors for automatic collision avoidance and with a graphical user interface to simulate the robot's movements. This makes it possible to check for possible collisions before the real execution of the movement.

During keyhole neurosurgery, robot and target poses could change, e.g., during SEEG procedures, in which up to 18 electrodes are implanted in the brain, generally in a single hemisphere. We have showed that, irrespective of the target pose, the robot can reach the target with the required accuracy, provided there is a clear line of sight between the markers attached on the end effector and the optical tracker (otherwise the robot is stopped). We also showed that convergence is robust with respect to angular error in the calibration matrix ($\theta < 50°$). The proposed approach is clinically relevant since it allows for the accurate positioning of the surgical instruments in the planned pose without modifying the robot controller, which is not accessible in commercially available devices. The final targeting accuracy achieved is that used by the external sensor.

Future work will be directed towards increasing the safety of the system so that the chosen path towards the target is clear of obstacles. Performance analysis of electrodes' positioning during SEEG in a real operating environment will also be carried out.

6. Acknowledgments

7. References

[1] A. Lanfranco, A. Castellanos, J. Desai, and W. Meyers, "Robotic surgery - a current perspective," Annals of Surgery,, vol. 239, no. 1, pp. 14–21, Jan. 2004.

[2] M. J. Lee and E. L. Lin, "The use of the three-pronged mayfield head clamp resulting in an intracranial epidural hematoma in an adult patient," European Spine Journal, vol. 19, pp. 187–189, 2010.

[3] J. Jin, S. Ryu, J. Rock, K. Faber, M. Gates, S. Li, and B. Movsas, "Image-guided target localization for stereotactic radiosurgery: accuracy of 6D versus 3D image fusion," Radiosurgery-Basel, vol. 6, p. 50, 2006.

[4] Shamir, Reuben R., et al. "Localization and registration accuracy in image guided neurosurgery: a clinical study," International Journal of Computer Assisted Radiology and Surgery, 4.1, pp. 45-52, 2009.

[5] M. Shoham, M. Burman, L. Joskowicz, E. Batkilin, and Y. Kunicher, "Bone-mounted miniature robot for surgical procedures: Concept and clinical applications," IEEE Transaction on Robotics and Automation, vol. 19, no. 5, pp. 893–901, Oct. 2003.

[6] W. Sukovich, S. Brink-Danan, M. Hardenbrook, "Miniature robotic guidance for pedicle screwplacement in posterior spinal fusion: early clinical experience with the SpineAssist®," The International Journal of Medical Robotics and Computer Assisted Surgery, no. 2, pp. 114–122, 2001.

[7] L. Joskowicz, R. Shamir, M. Freiman, M. Shoham, E. Zehavi, F. Umansky, & Y. Shoshan, "Image-guided system with miniature robot for precise positioning and targeting in keyhole neurosurgery", Computer Aided Surgery, 11, no. 4, pp. 181-193, 2006.

[8] F. Cardinale, M. Cossu, L. Castana, M. Schiariti, A. Miserocchi, G. Casaceli, C. Caborni, A. Moscato, and G. Lo Russo, "Five hundreds stereoelectroencephalography (SEEG) procedures for epilepsy surgery: a retrospective analysis of clinical safety and in vivo application accuracy," in International Journal of Computer Assisted Radiology and Surgery, Volume 7, Issue 1, pp. 124–125, Jun 2012.

[9] C. M. Oliveira, H. T. Nguyen, A. R. Ferraz, K. Watters, B. Rosman, and R. Rahbar, "Robotic surgery in otolaryngology and head and neck surgery: A review," Minimally Invasive Surgery, vol. 2012, pp. 1–11, 2012.

[10] C. J. Coulson, A. P. Reid, D. W. Proops, and P. N. Brett, "ENT challenges at the small scale," The International Journal of Medical Robotics and Computer Assisted Surgery, vol. 3, no. 2, pp. 91–96, 2007.

[11] S. Nishihara, N. Sugano, T. Nishii, H. Tanaka, N. Nakamura, H. Yoshikawa, and T. Ochi, "Clinical accuracy evaluation of femoral canal preparation using the ROBODOC system," Journal of Orthopaedic Science, vol. 9, no. 5, pp. 452–461, 2004.

[12] R. Tarwala and L. D. Dorr, "Robotic assisted total hip arthroplasty using the MAKO platform," Current Reviews in Musculoskeletal Medicine, vol. 4, no. 3, pp. 151–156, 2011.

[13] S. D. Chang, W. Main, D. P. Martin, I. Gibbs, and M. P. Heilbrun, "An analysis of the accuracy of the CyberKnife: a robotic frameless stereotactic radiosurgical system," Neurosurgery, vol. 52, no. 1, pp. 140–147, 2003.

[14] R. Horaud and F. Dornaika, "Hand-eye calibration," The International Journal of Robotics Research, vol. 14, no. 3, pp. 195–210, 1995.

[15] K. Daniilidis, "Hand-eye calibration using dual quaternions," The International Journal of Robotics Research, vol. 18, no. 3, pp. 286–298, 1999.

[16] I. Fassi and G. Legnani, "Hand to sensor calibration: A geometrical interpretation of the matrix equation $A \cdot X = X \cdot B$," Journal of Robotic Systems, vol. 22, no. 9, pp. 497–506, 2005.

[17] K. H. Strobl and G. Hirzinger, "Optimal hand-eye calibration," in Proceedings of the 2006 IEEE/RSJ International Conference on Intelligent Robots and Systems (IROS, Beijing), pp. 4647–4653, 2006.

[18] E. De Momi, P. Cerveri, E. Gambaretto, M. Marchente, O. Effretti, S. Barbariga, G. Gini, and G. Ferrigno, "Robotic alignment of femoral cutting mask during total knee arthroplasty," International Journal of Computer Assisted Radiology and Surgery, vol. 3, no. 5, pp. 413–419, 2008.

[19] J. Cornellà, O. J. Elle, W. Ali, and E. Samset, "Improving cartesian position accuracy of a telesurgical robot," in IEEE International Symposium on Industrial Electronics, pp. 1261–1266, 2008.

[20] M. D. Comparetti, A. Vaccarella, I. Dyagilev, M. Shoham, G. Ferrigno, and E. De Momi, "Accurate multi-robot targeting for keyhole neurosurgery based on external sensors monitoring," Proceedings of the Institution of Mechanical Engineers, Part H: Journal of Engineering in Medicine, vol. 226, no. 5, pp. 347–359, May 2012.

[21] P. Morgan, T. Carter, S. Davis, A. Sepehri, J. Punt, P. Byrne, A. Moody, and P. Finlay, "The application accuracy of the pathfinder neurosurgical robot," in International Journal of Computer Assisted Radiology and Surgery, ed. H. U. Lemke, K. Inamura, K. Doi, M. W. Vannier, A. G. Farman, and J. H. C. Reiber,, vol. 1256, pp. 561–567, 17th International Congress and Exhibition of Computer Assisted Radiology and Surgery, London, England, June 25-28,2003,

[22] M. S. Eljamel, "Validation of the PathFinderTM neurosurgical robot using a phantom," The International Journal of Medical Robotics and Computer Assisted Surgery, vol. 3, no. 4, pp. 372–377, 2007.

[23] T. Haidegger, P. Kazanzides, B. Benyo, and Z. Benyo, "Event-based patient motion detection and compensation in image-guided robotics," in IEEE RAS & EMBS International Conference on Biomedical Robotics and Biomechatronics, pp. 841–846, 2012.

[24] Xiang Yi and Robert Bicker, Design of a robotic transcranial magnetic stimulation system. Diss. University of Newcastle upon Tyne, 2012.

[25] Lars Richter et al., "Robust real-time robot-world calibration for robotized transcranial magnetic stimulation," The International Journal of Medical Robotics and Computer Assisted Surgery, 7.4, pp. 414-422, 2011.

[26] M. D. Comparetti, E. De Momi, A. Vaccarella, M. Riechmann, and G. Ferrigno, "Optically tracked multi-robot system for keyhole neurosurgery," in Proceedings of the 2011 IEEE International Conference on Robotics and Automation (ICRA, Shanghai), pp. 661–666, May 2011.

[27] J. B. West and C. Maurer, "Designing optically tracked instruments for image-guided surgery," IEEE Transactions on Medical Imaging, vol. 23, no. 5, pp. 533–545, May 2004.

[28] R. Bischoff, J. Kurth, G. Schreiber, R. Koeppe, A. Albu-Schäffer, A. Beyer, O. Eiberger, S. Haddadin, A. Stemmer, G. Grunwald et al., "The KUKA-DLR lightweight robot arm. a new reference platform for robotics research and manufacturing," in 41st International Symposium on Robotics (ISR) and 6th German Conference on Robotics (ROBOTIK), pp. 1–8, 2010.

[29] T. Xia, C. Baird, G. Jallo, K. Hayes, N. Nakajima, N. Hata, and P. Kazanzides, "An integrated system for planning, navigation and robotic assistance for skull base surgery," International Journal of Medical Robotics and Computer Assisted Surgery, vol. 4, no. 4, pp. 321–330, Dec. 2008.

[30] Q. Li, L. Zamorano, A. Pandya, R. Perez, J. Gong, and F. Diaz, "The application accuracy of the Neuromate robot - a quantitative comparison with frameless and frame-based surgical localization systems," Computer Aided Surgery, vol. 7, no. 2, pp. 90–98, 2002.

[31] O. Bebek, M. Hwang, and M. C. Cavusoglu, "Design of a parallel robot for needle-based interventions on small animals," IEEE/ASME Transactions on Mechatronics, vol. 18, no. 1, pp. 1–12, 2011.

[32] M.S. Eljamel, "Robotic neurological surgery applications: accuracy and consistency or pure fantasy?" Stereotactic and Functional Neurosurgery, 87(2), pp. 88-93, 2009.